Cooperative Research on Rotor Blade Optimization between JAXA-ONERA-DLR: Results of Phase I

KIMURA Keita, SUGIURA Masahiko, SUGAWARA Hideaki, TANABE Yasutada
(Japan Aerospace Exploration Agency)
Gunther Wilke (DLR: German Aerospace Center)
Joëlle Bailly (ONERA: The French Aerospace Lab)
TAKEKAWA Kuniyuki (Ryoyu Systems)

ABSTRACT

A collaborative research on optimization of a main rotor blade for helicopters by JAXA, ONERA and DLR is underway. As a first step, blade optimization method with five design variables is explored by dealing with hovering conditions. Optimizations and simulations are carried out by each agency with their own analysis codes and these results are cross-validated. This paper presents an overview of the project and an interim report on the results obtained so far.

1. Introduction

Helicopter blade design has advanced dramatically over the past decade with the rise of optimization tools. The three organizations, JAXA, ONREA and DLR, have been engaging in the research and development of the blade optimization methodologies based on multi-fidelity analytical tools for multi-objectives. A collaborative study is currently underway to share knowledge and recommendations for best practice guidelines on single- and multi-objective optimization methods for aerodynamic and acoustic design as applied to rotor design. As the phase I of this trilateral study, we compared and verified the multi-fidelity analytical tools and the optimizers in each agency.

In the field of high-fidelity aerodynamic rotor blade optimization, there are currently two major routes observed: The first approach relies on gradient based optimizations, where the computational fluid dynamics (CFD) solution is adjoint to cost-effectively retrieve the flow gradients. Recent examples are given by Fabiano and Mavriplis [1] and Wang et al. [2]. Both of these examples optimize the HARTII rotor using 95 and 79 design variables. As opposed to the gradient based approach, which may be difficult for multi-objective optimization, the surrogate based approach allows handling multiple functions independently of each other. The idea of the surrogate model is to approximate the simulation code through simple mathematical relations. This allows us to quickly search the optimal location in the surrogate model to find the optimum. Often, this approach is applied iteratively, where the surrogate model is successively improved by adding more samples to it. This is the fundamental idea of the EGO algorithm [3]. All three partners have applied their versions of this approach in the past and thus these are briefly reviewed for the second optimization approach.

In JAXA, optimization studies of blade shape have been conducted basically based on high-fidelity CFD last few years [4] [5] [6]. Thanks to the Kriging surrogate model, optimizations have been successful with a small number of simulations necessary. Most recently, JAXA has improved blade designs in forward flight with high advance ratios using numerical optimization. [7]

Since the last decade, ONERA has developed aerodynamic optimization procedures including low fidelity and high fidelity, thanks to the development of surrogate models based on Kriging and Co-Kriging methodologies. ONERA and JAXA set up their own optimization procedures based on Kriging methodology conducting CFD calculations for a hover configuration [4]. More recently, for an advancing flight configuration, Bailly [8] has shown the importance of taking into account three-dimensional unsteady effects to correctly design a complex geometry blade planform (with sweep evolutions), thanks to Co-Kriging method used in the optimization procedure. This methodology appeared very efficient to design a realistic blade, with a limited number of CFD computations (based on CDS/CFD coupling).

On the DLR side, aerodynamic rotor optimization using high-fidelity CFD dates back to the works by Imiela [9]. He was among the first to perform fluid-structural coupled simulations during the optimization and proved that a different rotor may be obtained if not considered. This approach has been successfully applied Imiela and Wilke [10]. As the overall computational cost of the optimization is still high despite the acceleration using surrogate models, Wilke [11] adopted a methodology to incorporate data from simulations of different fidelities to accelerate the approach, which could reduce the cost of the optimization by up to 69%. He enhanced the optimization process to cope with multiple objectives to retrieve a Pareto front.

In this paper, the results of phase I of the cooperative research to date are summarized. That includes the cross-validation of the performance prediction accuracy of the low/high-fidelity analysis tools and optimization algorithms owned by each agency.

2. Optimization methodologies

2.1. JAXA

JAXA uses a Genetic Algorithm (GA) optimization within the Kriging surrogate model. The Kriging model can model not only the distribution of the function values themselves but also the uncertainties that may be included in the estimated function values using algebraic expressions.

An index called Expected Improvement (EI) is employed to evaluate the location of the next sample point. The EI balances the actual prediction value and surrogate model error to exploration and exploitation. In the EGO [3] method, the response surface is reconstructed by adding new sample points that are likely to be better than the current value. More detailed settings of the GA and Kriging model are noted in the references [12),13)].

2.2. ONERA

ONERA has developed the KORRIGAN in-house code which can build Kriging and Co-Kriging surrogate models [8)]. The Kriging methodology is based on the statistical interpolation method suggested by Krige[14)], and mathematically studied by Matheron[15)]. Within the framework of this study, the Gaussian kernel is chosen as the correlation function. The internal parameters of this function are determined by a genetic algorithm implemented in the code. This GA is also used to search for the minimum of the model, and for the maximum of the Expected Improvement (EI) [16)], thanks to an Efficient Global Optimization (EGO) algorithm. The sampling is enriched by the real evaluation of these points, to improve the accuracy of the model.

The idea of the Co-Kriging is to use all available information to estimate unknown high-fidelity simulation. The basic Kriging formulation has been extended by many authors to combine multiple levels of simulation to create a more accurate or less expensive high fidelity model. ONERA used the Kennedy and O'Hagan approach [17)], based on an auto-regressive model which consists in approximating the high fidelity model by multiplying the low fidelity model by a scaling factor, and by adding a Gaussian process representing the difference between the low and high fidelity data. As for the Kriging procedure, the sampling data are updated with real high-fidelity estimations of the goal function successively for the minimum point of the model, and the maximum of the Expected Improvement point.

2.3. DLR

The method applied here is also based on the EGO approach by Jones et al. [3)] and has been implemented into the in-house Powerful Optimization Toolkit with Surrogate Models (POT with SuMo) [11)]. A hybrid optimization to find the maximum Expected Improvement is used. First the Differential Evolutionary algorithm by Storn and Price is started [18)], which locates the global optimum. It is then further refined with the Simplex algorithm by Nelder and Mead [19)]. Failing rotor designs are handled through the 'crashmap' approach. Instead of using a penalty function in the goal function surrogate model, a separate surrogate model is used which simply records whether the design has been successful or not. When searching for the Expected Improvement, it is then multiplied with the probability that the simulation will be successful. In this scenario, untrimmable rotor configurations have been considered as failed designs. By using the crashmap approach, a failed simulation is only inserted into the constraint surrogate model, but not into the goal function surrogated model, where only successful designs are recorded, keeping it untainted.

3. Simulation Methodologies

In the process of optimization, a method to evaluate its aerodynamic performance is necessary, and simulations of various fidelity levels will be used. In this study, two levels of simulation, low-fidelity and high-fidelity, are used to evaluate and optimize the aerodynamic performance. In this section, details about the simulation tools of each agency are provided.

3.1. Low-fidelity method

3.1.1. JAXA

JAXA has developed a simple analysis method for rotor performance based on blade element momentum (BEM) theory. The aerodynamic forces are calculated by finding the angle of attack based on the twist angles at each blade span position and the inflow direction, and by referring to the airfoil look-up table for the corresponding drag and lift coefficients. From the calculated aerodynamic forces, the induced velocities on the rotational plane are calculated using the momentum relation and feedback is iterated until converged. The blade lead-lag motion is set to zero and the elastic deformation of the blade is not considered.

3.1.2. ONERA&DLR

Both ONERA and DLR performed low-fidelity simulations with the HOST comprehensive code developed by Airbus Helicopter[20)]. The elastic model uses the assumptions of a long and slender beam, discretized along the pitch axis as an assembly of rigid segments with the elastic properties contained in the joints connecting them. The induced velocities are modeled with the finite state inflow model, called FiSuW [21)], developed at ONERA.

During the optimization procedure, the blade planform is modified, leading to a change of the structural data (mass, inertia, stiffness par unit of length). ONERA developed an updating procedure of these structural data [22)], based on analytical polynomial laws that describe the evolutions of the stiffnesses, the mass and the inertia per unit length with respect to the chord and the thickness distributions of the profiles of the blade. Some analytical corrections are also performed to adjust the elastic axis and the gravity center axis with respect to the pitch axis.

3.2. High-fidelity simulations (CFD)

The high-fidelity simulations are carried out by using CFD solvers developed by each agency. From the point of view of computational cost and sufficient accuracy, (U-)RANS (Unsteady Reynolds averaged Navier-Stokes) was chosen to carry out the simulations. Table 1 shows a summary of the CFD conditions adopted by each agency in this study.

Each agency has a different CFD solver. So it is necessary to prepare a computational grid of comparable quality to obtain consistent results. Certain mesh standards have been agreed upon, while the final implementations of them are given in Table 2.

Table 1 : Main difference of CFD methods between each agency

	JAXA (rFlow3D)	ONERA (elsA)	DLR (FLOWer)
Spatial order	4th order FCMT+SLAU	2nd order cell-center Jameson	4th order FMCT (vA) + SLAU2
Time integration	LU-SGS 4 stage RK	Implicit Euler scheme + Gear sub-iterations	5 stage RK + implicit residual smoothing
Turbulence model	SA-R	Kok-SST	SA-R + Empirical Transition
Rotor deformation	Rigid	Elastic	Elastic
Grid setting	Chimera (blade+background)	Chimera (blade+background) Periodic	Monocoque (single blade periodic)

Table 2 : Grid settings used by each partner

	JAXA	ONERA	DLR
Grid points in chordwise direction	161	218	161
Grid points in spanwise direction	121	194	161
Grid points in boundary layer	~50	~35	~ 35-60
Y+ of the first cell in the boundary layer	< 1	≤1	~ 1
Farfield distance above the rotor	100R	6R	6R
Farfield distance below the rotor	100R	6R	6R
Farfield distance in radial direction	100R	6R	2.5R
Grid resolution far wake region in chord length	20% in all directions	9~100% circumferential 11% vertical 8% radial	100% circumferential 13 % vertical 9 % radial
Total # of cells	16 M	10.3 M	4.4 M

3.2.1. JAXA : rFlow3D

The CFD Solver for rotorcraft (rFlow3D) has been developed in JAXA. The governing equations are the compressible Navier–Stokes equations, which are discretized using a finite volume method. By adopting the moving overlapped grid, rotational movement of blades can be solved directly. By coupling an all-speed scheme mSLAU [23] and 4th order spatial scheme FCMT [24], low dissipation calculations are achieved over a wide Mach number range. The total forces and moments in each spatial direction are trimmed. Basically, a Chimera grid setup with a background grid and a moving blade grid is used for calculations. For time integration, a 4 stage Runge-Kutta is adopted for the background grid and a dual-stepping LU-SGS implicit method is used for the blade grids. The Spalart-Allmaras turbulence model with rotational correction (SA-R) [25] is used as the turbulence model for the RANS closure.

3.2.2. ONERA : elsA

The High fidelity computations are performed using a loose coupling procedure between the HOST comprehensive analysis code [20] and the CFD solver developed at ONERA, called elsA [26]. The HOST calculations provide the trim and the elastic deformations to the elsA code, which feeds back a three-dimensional correction on the airloads to HOST. The three dimensional unsteady Navier-Stokes equations are solved by the cell-centered second-order Jameson's scheme. The time integration is performed by an implicit Euler scheme with Gear sub-iterations. The time step is equivalent to 1 deg of blade rotation. The turbulence model is Kok's k-Ω [27] with Mentor's shear-stress transport (SST) corrections [28]. The flow is assumed to be fully turbulent. The grids are generated using the Chimera technique. A multiblock deformable mesh of O-H type is generated around an isolated blade, containing almost 3 million points. This mesh is immersed in a background quarter cylinder grid, containing 7.3 million points. The total mesh contains 10.3 million points (considering an isolated blade). The following boundary conditions are applied on the different surfaces of the quarter cylinder : inviscid wall conditions on the internal surface, Froude conditions on the external, lower and upper surfaces to limit the recirculation areas in the computational domain, and periodic conditions on the lateral surfaces.

3.2.3. DLR : FLOWer

The legacy CFD solver FLOWer [29] is applied here. A first order dual time stepping approach is utilized with a 5 stage Runge-Kutta scheme using implicit residual smoothing. The spatial discretization of the inviscid fluxes is similar to JAXA's approach: The SLAU2 scheme by Kitamura et al. [23] is applied with the 4th order FMCT reconstruction by Yamamoto et al. [24]. To further reduce numerical dissipation, the minmod limiters have been exchanged with van Albada type limiters. The chosen turbulence model is SA-R by Dacles-Mariani et al. [25]. Empirical transition criteria employed as suggested by Heister [30].

The CFD simulations are fluid structurally coupled and the whole process is depicted in Figure 1. The in-house grid generation G3 generates a monocoque periodic rotor mesh using transfinite interpolation. Then, HOST is called to compute an initial trim state and deformations, which are then coupled with FLOWer airloads using the delta airloads approach [31].

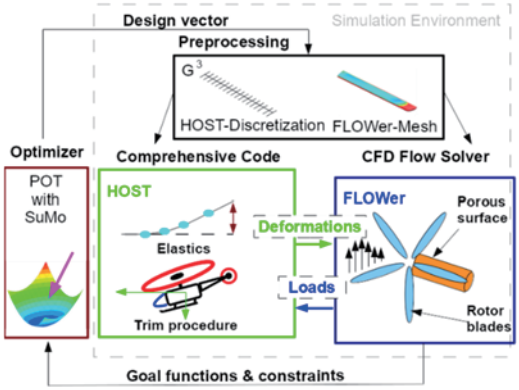

Figure 1: DLR's rotor optimization process

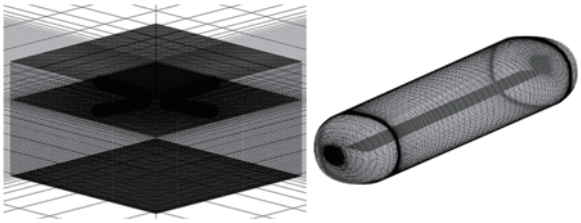

JAXA (chimera, 2 backgrounds + blade)

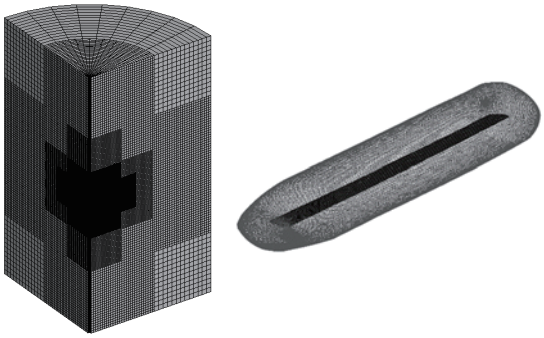

ONERA (chimera, 1/4 periodic BK + blade)

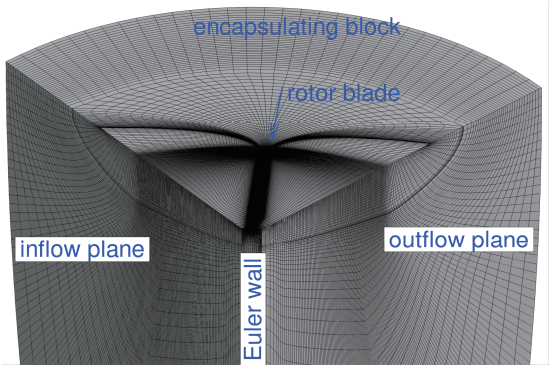

DLR (split in the middle)

Figure 2 : CFD grid around blade

3.3. Reference rotor test

The blade of the HART II test [32] was used for the baseline simulation and optimization. The experimental setup of HART II is described in Table 3. In this test, 40% down-scaled model of the Bo105 main rotor was investigated in the open jet test section of DNW (German-Dutch Wind Tunnels).

Table 3 : Specifications of HART II rotor [32]

Number of blades	4
Airfoil section	Modified NACA23012
Radius R [m]	2.0
Solidity σ	0.077
RPM	1042
Tip Mach number M_{tip}	0.641
Root cutout [m]	0.44
Chord length c_{ref} [m]	0.121

4. Baseline simulations

The accuracy of the BEM and CFD simulations were cross-validated through the analysis of the HARTII rotor described in chapter 3. In this study, the hovering condition were analyzed and compared with the figure of merit.

4.1. Low-Fidelity Methods

The changes in thrust T and torque Q of the HARTII rotor through the collective pitch angle sweep are organized in Figure of merit (FoM), which is the hovering efficiency. The formulation is shown in Eq. 1 and Eq. 2. Where, a_∞ is the speed of sonic, $\mathrm{C_T}$ and $\mathrm{C_Q}$ are thrust and torque coefficients.

$$\mathrm{C_T} = \frac{T}{\rho\pi R^2 a_\infty^2 M_{tip}^2}, \quad \mathrm{C_Q} = \frac{Q}{\rho\pi R^3 a_\infty^2 M_{tip}^2} \qquad \text{Eq. 1}$$

$$\mathrm{FoM} = \frac{C_T^{1.5}}{\sqrt{2}\, C_Q} \qquad \text{Eq. 2}$$

The thrust-FoM curve is summarized in Figure 3. The thrust is expressed as thrust per blade area using solidity. The design thrust ($\mathrm{C_T}/\sigma = 0.1$) to be optimized in this study is illustrated as an auxiliary line. The overall trends in the analyses are similar, and the design thrust values of FoM are 66.9% for JAXA, 65.4% for DLR and 67.6% for ONERA, respectively. Compared with the experimental data [33], the tendency of overestimation was observed in each case with small thrust conditions. This is especially noticeable in JAXA's case and it is partly due to the fact that an ideal flow tube is assumed in BEM that does not take the presence of blades into account.

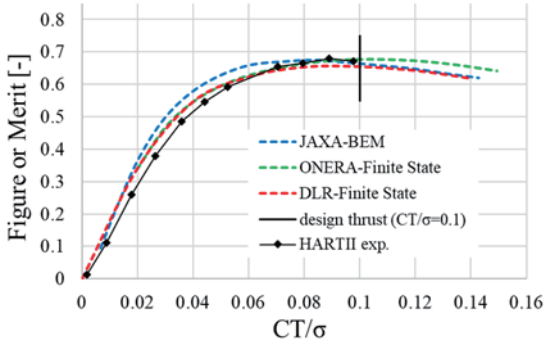

Figure 3 : Figure of Merit by Low-Fidelity methods (Experimental data are from[33])

The distribution of the thrust in the spanwise direction is

compared using the blade loading coefficient C_nM^2, which is defined in Eq. 3, where N is the normal force acting on the blade element, c represents chord length and dr is width at each radial location.

$$C_nM^2 = \frac{N}{\frac{1}{2}\rho a_\infty^2 cdr} \qquad \text{Eq. 3}$$

Figure 4 shows a comparison of C_nM^2 distributions under the design thrust condition ($C_T/\sigma = 0.1$). Almost identical solutions are obtained for the region from root cut (r/R=0.22) to r/R~0.9, indicating that the difference in FoM shown earlier is caused by the treatment near the blade tip. The JAXA BEM code assumes a rigid rotor, while the HOST code used in DLR and ONERA takes into account the elastic deformation of the beam model. This shows that for the present rotor, the elastic deformation has small influence on the performance.

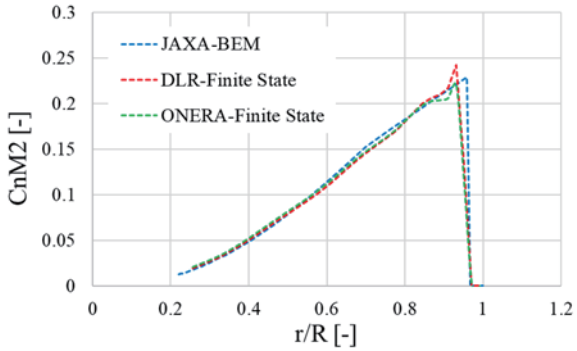

Figure 4 : Blade loading coefficient C_nM^2 (by BEM)

4.2. CFD

As with the low-fidelity methods, the Figure of Merit of the hovering condition was calculated by CFD and is shown in Figure 5. In addition to the design thrust of C_T/σ=0.1, the target thrust was set in increments of 0.02, and calculations were carried out at each agency. Figure 5 shows good agreement over a wide range from C_T/σ=0.02 to 0.1 of the design thrust. On the other hand, in the range C_T/σ>0.1, the collective pitch of the blade is large, it reaches detached flow condition and quantitative differences can be seen. Despite the same turbulence model applied between JAXA and DLR, a clear difference is seen in the thrust range. However, the result of ONERA shows a trend similar to that of JAXA, regardless of the different turbulence closure. As will be discussed later, the difference between DLR and JAXA for the high thrust ranges may arise from the different vortex preservation. The stronger vortex preservation of DLR leads to a strong separation at the blade tip past the design point, which is less severely captured by JAXA. Normally, the grid resolution is relatively coarse for CFD based evaluation for optimization to avoid increased computational cost, and the results in such detached points are likely to have many uncertainties. This should be kept in mind when setting the target operating conditions for the optimization. The design thrust values of FoM are 67.9% for JAXA, 68.9% for DLR and 65.0% for ONERA, respectively.

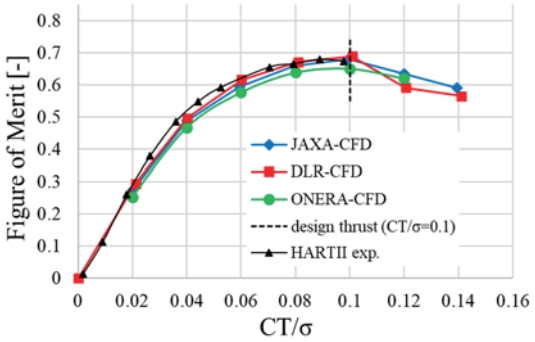

Figure 5 : Figure of Merit by CFD (Experimental data are from [33])

The blade loading distributions were then checked to further discuss the differences in CFDs for each agency under the target thrust condition of $C_T/\sigma = 0.1$ (Figure 6). The peaks are found at 95% of the span in all CFD cases, with the DLR and ONERA cases being in good agreement and the JAXA case having slightly smaller value. In the 80~90% of the span, the JAXA and ONERA cases gain more thrust than the DLR. In addition, the ONERA case has smaller values than the other two agencies in the low speed region near the root of the DLR.

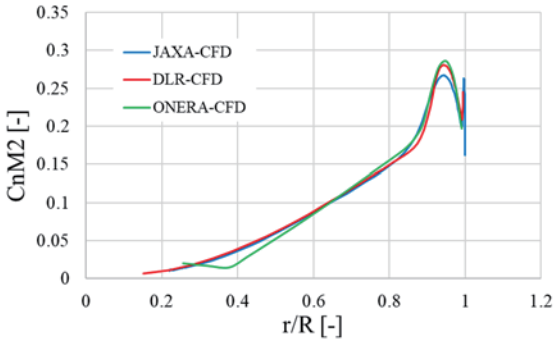

Figure 6 : CnM2 spanwise distribution (in design point $C_T/\sigma = 0.1$)

One of the uncertainties included about the aerodynamic performance near the blade tip should be the effect of tip vortex interference. Figure 7 shows a visualization of the tip vortices generated from the blade (In C_T/σ=0.1) in terms of vorticity. The tip vortices generated from the previous blade passed around r/R~0.9. The smaller peak of C_nM^2 in JAXA's case in Figure 6 may be due to the relatively small resolved vorticity. JAXA used coarse resolution of the background grid of the vortices, where resolution was 0.2 times of the blade chord. Furthermore, the adoption of the chimeric grid system reduced the vorticity due to data interpolation between the coarse background grid and the blade grid.

On the other hand, ONERA uses a higher background grid resolution and DLR adopts a single quarter-periodic grid, which results in a higher resolution. Assuming comparable computational cost per grid point, the monocoque periodic meshing approach has advantages of preventing the decay of vorticity because there is no interpolation of data between grids and a higher resolution is attained for the same number of grid points.

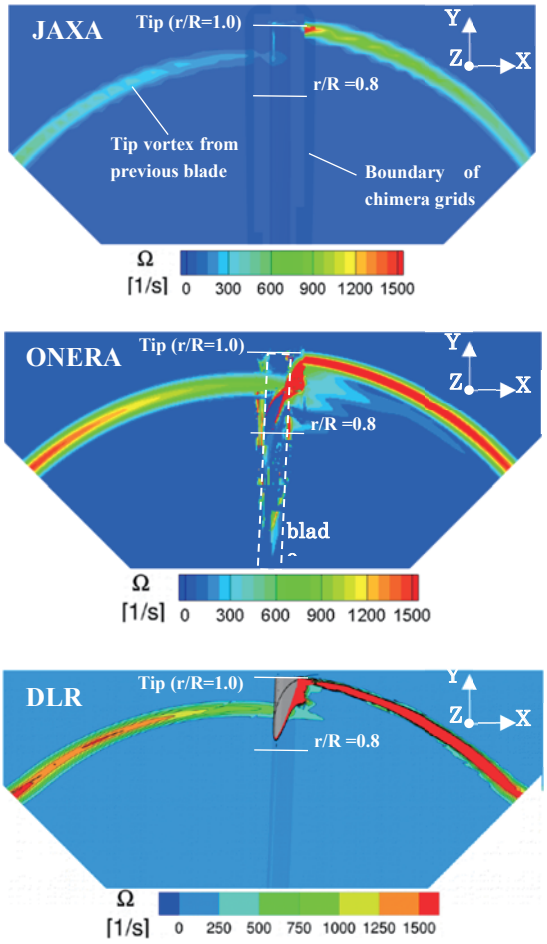

Figure 7 : Vorticity contour in 1/4 rotational plane at Z = 0.1m under design thrust condition (C_T/σ = 0.1)

Furthermore, the distribution of the blade loading is investigated from the distributions of pressure coefficient C_p and skin frictional coefficient C_f on the blade surface at r/R=0.87 as the representative span position (Figure 8). The horizontal axis takes the chord direction coordinates from the leading edge and is normalized by chord length. The definition of each is shown in Eq. 4. They are normalized by dynamic pressure at each span position,

$$C_p = \frac{P}{\frac{1}{2}\rho a_\infty^2 M_{sec}^2} \qquad C_f = \frac{\tau}{\frac{1}{2}\rho a_\infty^2 M_{sec}^2} \qquad \text{Eq. 4}$$

where M_{sec} is the local Mach number at the section. These distributions show a significant difference in the use of the turbulence model between JAXA and ONREA, which are calculated under fully turbulent conditions, and DLR, which used an empirical transition model.

Especially in the region of x/c<0.2, the skin friction in the DLR case is noticeably smaller than the other two, and the same trend is observed as the trailing edge is approached, which indicates that the application of laminar flow calculation through the use of the transition model reduces the overall predicted torque. That is the main reason for higher FoM than JAXA and ONERA's case.

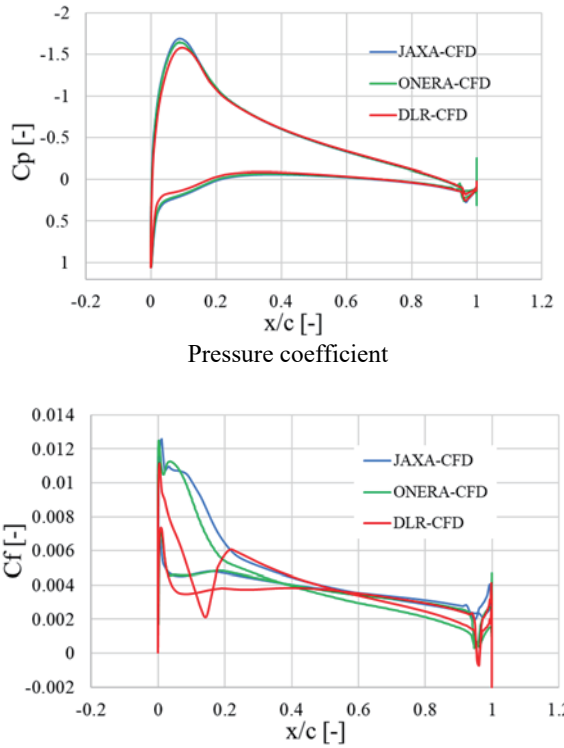

Pressure coefficient

Skin frictional coefficient

Figure 8 : Chord wise aerodynamic distribution at r/R=0.87 under design thrust condition (C_T/σ = 0.1)

5. Rotor optimization

5.1. Optimization parameters

When considering the design of the blade shape, there is a wide variety of design variables which include chord length, twist, dihedral/anhedral and forward/backward sweep angles. In addition, these variables are usually distributed with respect to the blade span, so there is an almost infinite number of conditions.

Therefore, it is important to set up search conditions that allow the objective function to vary significantly with fewer design variables in order to solve the optimization problem. For the hovering condition, the objective function is the hovering efficiency (Figure of Merit).

In this study, the twist and the chord length at radial positions are used as design variables that have a significant impact on the hovering performance. This limits the degrees of freedom. Cubic spline interpolation is applied for the parameterization. The design variables are summarized and shown in Table 4 and Figure 9.

Table 4 : Design variables

Variables	Control Points	Constraints
θ_1	r/R = 0.875	-5~5°
θ_2	r/R = 1.0	-10~10°
r_c	-	0.65~0.85R
c_1	r = r_c	1.0~1.5c_{ref}
c_2	r/R = 1.0	0.5~1.0c_{ref}

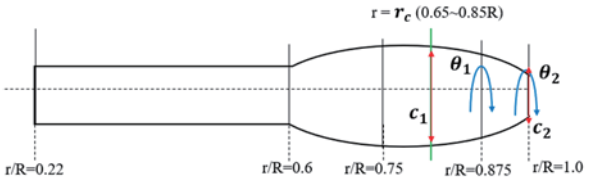

Figure 9 : Design variables for optimization

5.2. Optimization results

An exterior view of the planar shape of the blades derived by each agency is shown in Figure 10. All partners retrieve a similar blade design.

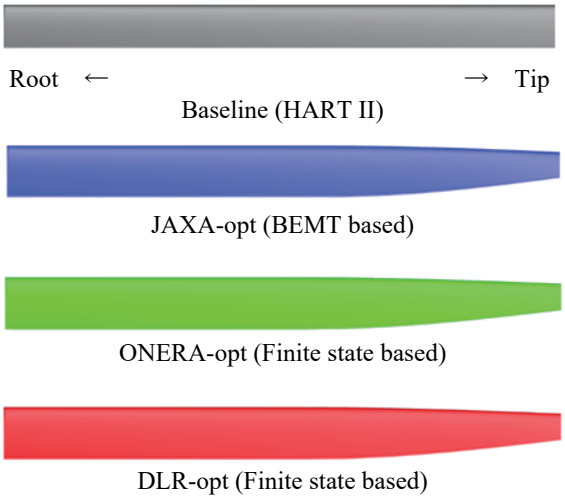

Figure 10 : Optimized shape by each agency

The values of the design variables derived from each agency's optimization tool are shown in Table 5 and the chord length and twist angle distributions obtained through the spline interpolation are shown in Figure 11.

The chord length distributions are almost identical with only a slight difference in the design target section position r_c. The twist angle distributions are consistent with the trend that the twist angle is sharply decreased toward the blade tip, with values of -4.7° at the tip for ONERA, -5.7° for DLR and -8.1° for JAXA. The larger value in the case of JAXA seems to be the effect calculated in the rigid rotor condition as well as the use of a different inflow model. When the angle of attack is a positive value, the pitching moment lowers the pitch angle and thus the elastic twist of -1.8° adds on top of the rigid twist for DLR and ONERA.

Table 5 : Design variables derived by optimization (based on low-fidelity methods, values are rounded off)

Variables	JAXA	ONERA	DLR
θ_1	-1.3°	-0.85°	-0.54°
θ_2	-8.1°	-4.5°	-5.7°
r_c	0.68	0.65	0.65
c_1	1.0	1.0	1.0
c_2	0.5	0.5	0.5

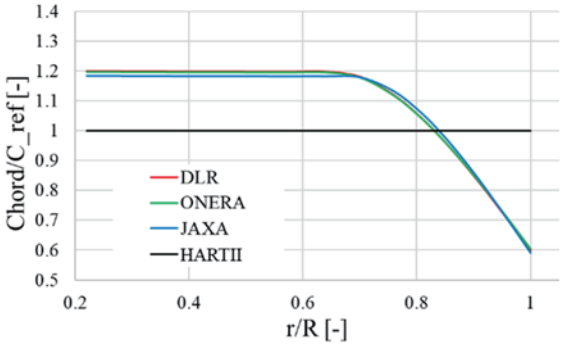

Chord length

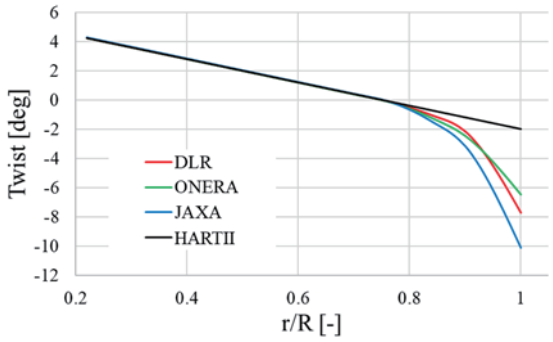

Twist angle

Figure 11 : Span-wise distribution of twist and chord length

Finally, the Figure of Merit of optimized shape and their improvements from the baseline shape in design thrust are shown in Figure 12 and Figure 13. There are no cases where the FoM in the baseline shape exceeded 0.7 in both BEM and CFD. However, in the optimized shapes, results exceeding 0.7 are confirmed over a wide range of thrust conditions. Comparison in the design thrust condition shows significant of hovering performance: 0.770 for JAXA, 0.770 for ONERA and 0.775 for DLR respectively.

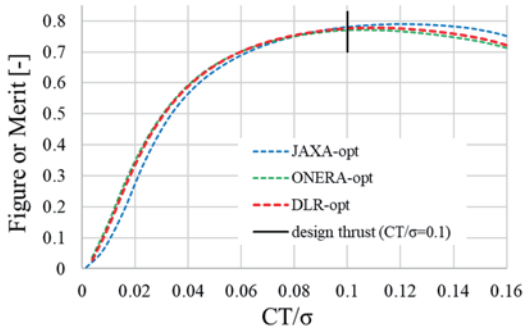

Figure 12 : Figure of Merit of optimized shape (by JAXA's BEMT)

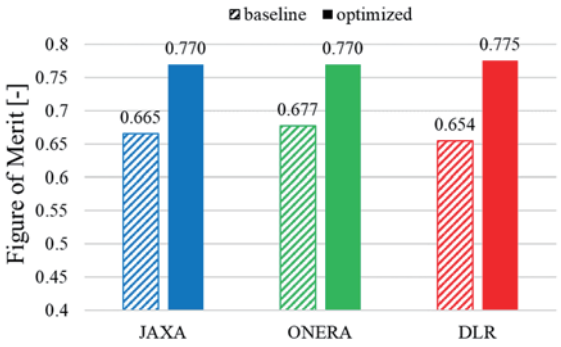

Figure 13 : Improvement of FoM at design point C_T/σ = 0.1 through optimization

6. Concluding remark

As the first step in the optimization study of helicopter blades by JAXA, DLR, and ONERA, mutual verifications were performed as for low-fidelity (BEMT and finite state) and high-fidelity (CFD) analytical tools and optimization algorithms. Through validation calculations using the HARTII rotor as a baseline, it is confirmed that the agencies' low-fidelity and CFD aerodynamic evaluation methods show similar trends under a wide range of thrust conditions. In addition, quantitative comparison of the analysis results confirmed the influence of differences in detailed condition settings on the aerodynamic evaluation tools such as elastic deformation, grid and turbulence modeling etc. in CFD. For the validation of the optimization tools, the hovering performance was optimized by using low-fidelity aerodynamic evaluation tools. As a result, almost identical blade planform geometries were obtained from each agency. This means that a comparative validation of both the optimization method and the analysis tool (BEM) was possible. Although the optimization using CFD as an evaluation tool was not performed at this time, it will be used in the future when optimizing the geometry with more complex parameters such as dihedral/anhedral and forward/backward sweep angles.

References

(1) E. Fabiano and D. Mavriplis, "Adjoint-Based Aeroacoustic Design-Optimization of Flexible Rotors in Forward Flight," *Journal of Americal Helicopter Society,* Vols. 62-4, pp. 1-17, 2017.

(2) L. Wang, B. Diskin, R. T. Biedron, E. J. Nielson, V. Sonneville and O. A. Bachau, "High-Fidelity Multidisciplinary Design Optimization Methodology with Application to Rotor Blades," *Journal of the American Helicopter Society,* 2019.

(3) D. R. Jones, M. Schonlau and W. J. Welch, "Efficient Global Optimization of Expensive Black-Box Functions," *Journal of Global Optimization,* vol. 13, pp. 455-492, 1998.

(4) M. Sugiura, Y. Tanabe, T. Aoyama, B. Ortun and J. Bailly, "An ONERA/JAXA Co-operative Research on The Assessment of Aerodynamic Methods for the Optimization of Helicopter Rotor Blades Phase II," 42th European Rotorcraft Forum, Lille, France, 2016.

(5) M. Sugiura, Y. Tanabe, H. Sugawara and M. Kanazaki, "Computationally Efficient and High Fidelity Optimization of Rotor Blade Geometry," 40th European Rotorcraft Forum, Southampton, UK, 2014.

(6) S. Takeda, M. Sugiura, Y. Tanabe, H. Sugawara, M. Kanazaki and M. Harigae, "Influence of Pre-twist Distribution at the Rotor Blade Tip on Performance during Hovering Flight," Transactions of the Japan for Aeronautical and Space Sciences, Vol. 58, No.1, pp.39-44, 2015.

(7) M. Sugiura, Y. Tanabe, H. Sugawara and K. Takekawa, "Optimal Design of Rotor Blade for a Winged Compound Helicopter at High Advanced Ratio," Vertical Flight Society Forum 76, Oct., virtual, (scheduled to be announced), 2020.

(8) J. Bailly and D. Bailly, "Multifidelity Aerodynamic Optimization of a Helicopter Rotor Blade," *AIAA Journal,* vol. 57, no. 8, pp. 3132 - 3144, 2019.

(9) M. Imiela, "High-fidelity optimization framework for helicopter rotors," *Aerospace Science and Technology,* vol. 23, pp. 2-16, 2012.

(10) M. Imiela and G. Wilke, "Passive Blade Optimization and Evaluation in Off-Design Conditions," in *39th European Rotorcraft Forum*, 2013.

(11) G. Wilke, "Variable-Fidelity Methodology for the Aerodynamic Optimization of Helicopter Rotors," *AIAA Journal,* vol. 57, pp. 3145-3158, 2019.

(12) M. Kanazaki, Y. Yokokawa, M. Murayama, T. Ito, S. Jeong and K. Yamamoto, "Nacelle Chine Installation Based on Wind-Tunnel Test Using Efficient Global Optimization," *Transactions of the Japan Society for Aeronautical and Space Sciences*,Vol. 51, No. 173, pp. 146-150, 2008.

(13) M. Kanazaki, S. Jeong and K. Yamamoto, "High-Lift System Optimization Based on Kriging Model Using High Fidelity Flow Solver," *Transaction of Japan Society for Aeronautical and Space Science*, Vol. 49, No. 165, 2006, pp. 169-174, 2006.

(14) D. Krige, "A Statistical Approach to Some Basic Mine Valuation, Problems in the Witwatersrand," *Journal of the Chemical Metallurgical and Mining Society of South Africa,* vol. 52, no. 6, pp. pp. 119-139, 1951.

(15) G. M. Matheron, "Principles of Geostatistics," *Society of Economic Geologists,* vol. 58, no. 8, pp. pp. 1246-1266, 1963.

(16) J. Sacks, W. J. Welch, T. Mitchell and H. Wynn, "Design and Analysis of Computer Experiments," *Statistical Experiments,* vol. 14, no. 4, pp. 409-423, 1989.

(17) M. Kennedy and A. O'Hagan, "Predicting the Output from a Complex Computer when a Cost Approximation is available," *Biometrika,* vol. 87, no. 1, pp. 1-13, 2000.

(18) R. Storn and K. Price, "Differential Evolution - A simple and efficient adaptive scheme for global optimization over continuous spaces," *Journal of Global Optimization,* vol. 11, pp. 341-359, 1997.

(19) J. A. Nelder and R. Mead, "A simplex function for minimization," *Computer Journal,* Vols. 8-1, pp. 308-313, 1965.

(20) B. Benoit, A.-M. Dequin, K. Kampa, W. von Grünhagen, P.-M. Basset and B. Gimonet, "HOST, a General Helicopter Simulation Tool for Germany and France," in *56th Annual Forum of the American Helicopters Society*, Virginia, 2000.

(21) P. Basset, O. Heuze, J. Prasad and M. Hamers, "Finite State Rotor Induced Flow Model for Interferences and Ground Efects," in *57th Annual Forum of the American Helicopter Society*, Washington (DC), 2001.

(22) J. Bailly, B. Ortun, Y. Delrieux and H. Mercier des Rochettes, "Recent Advances in Rotor Aerodynamic Optimization Including Structural Data Update," *Journal of the American Helicopter Society,* vol. 62, no. 2, pp. 1-11, 2017.

(23) K. Kitamura, E. Shima, K. Fujimoto and Z. J. Wang, "Performance of Low-Dissipation Euler Fluxes and Preconditioned LU-SGS at Low Speeds," *Communications in Computational Physics,* vol. 10, p. 90–119, 2011.

(24) S. Yamamoto, S. Kano and H. Daiguji, "An efficient CFD approach for simulating unsteady hypersonic shock-shock interference flows," *Computers & Fluids,* vol. 27, pp. 571-580, 1998.

(25) J. Dacles-Mariani, D. Kwak and G. Zilliac, "On numerical errors and turbulence modeling in tip vortex flow prediction," *International Journal for Numerical Methods in Fluids,* vol. 30, pp. 65-82, 1999.

(26) L. Cambier, S. Heib and P. Sylvie, "The ONERA elsA CFD Software : Input from Research and Feedback from Industry," *Mechanics and Industry,* vol. 14, no. 3, pp. 159-174, 2013.

(27) J. Kok, "Resolving the Dependance on Freestream Values for the k-Turbulence Model," *AIAA Journal,* vol. 38, no. 7, pp. 1292-1295, 2000.

(28) F. R. Mentor, "Two-equation Eddy-Viscosity Transport Turbulence Model for Engineering Applications," *AIAA Journal,* vol. 32, no. 8, pp. 1598-1605, 1994.

(29) J. Raddatz and J. K. Fassbender, "Block Structured Navier-Stokes Solver FLOWer," in *MEGAFLOW - Numerical Flow Simulation for Aircraft Design*, Berlin, 2005.

(30) C. C. Heister, "A Method for Approximate Prediction of Laminar-Turbulent Transition on Helicopter Rotors," *Journal of the American Helicopter Society,* vol. 63, pp. 1-14, July 2018.

(31) H. Yeo, M. Potsdam and R. Ormiston, "Application of CFD/CSD to Rotor Aeroelastic Stability in Forward Flight," in *66th Annual Forum of the American Helicopters Society*, 2010.

(32) B. vanderWall et al., "The HART II test in the LLF of the DNW - a major step towards rotor wake understanding," 28th European Rotorcraft Forum, Bristol, England, September, 2002.

(33) P. Küfmann, R. Bartels, B. vanderWall, O. Schneider, H. Holthusen, J. Gomes , and J. Postma, "The First Wind Tunnel Test of the DLR's Multiple Swashplate System: Test Procedure and Preliminary Results," Proceedings of the 72nd Annual Forum of the American Helicoper Society. American Helicopter Society Inc., 2016.